GMR
The Original

CISPLATIN-LOADED ZINC–POLYETHYLENE GLYCOL NANOPARTICLES EXHIBIT ENHANCED ANTICANCER EFFICACY AND REDUCED SYSTEMIC TOXICITY IN A MURINE MELANOMA MODEL

Mohsin Tajdar[1], Tahir Maqbool[1]*, Ayesha Sajid[2], Zulfiqar Ali Akram[2], Adnan Arshad[3]*, Muzammal Mateen Azhar[1], Awais Altaf[1]

[1] Institute of Molecular Biology and Biotechnology, The University of Lahore, Lahore, Pakistan
[2] Lahore Medical and Dental College, Lahore, Pakistan
[3] Forman Christian College University, Lahore, Pakistan

ABSTRACT

Background: Cisplatin remains a cornerstone chemotherapeutic agent; however, its clinical utility is constrained by dose-limiting nephrotoxicity, myelosuppression, and the emergence of drug resistance. Zinc–polyethylene glycol (Zn-PEG) nanoparticles offer a promising platform to overcome these limitations through enhanced tumor accumulation via the enhanced permeability and retention (EPR) effect, surface PEGylation-mediated immune evasion, and intrinsic zinc-mediated pro-apoptotic activity.

Objective: This study aimed to synthesize, physicochemically characterize, and evaluate the in vivo anticancer efficacy and systemic safety of cisplatin-loaded Zn-PEG nanoparticles (CIS/Zn-PEG NPs) in a syngeneic B16F10 murine melanoma model.

Methods: Nanoparticles were synthesized using a co-precipitation method by combining zinc acetate, PEG-2000, and sodium hydroxide under continuous stirring conditions. Subsequently, cisplatin was added gradually into the Zn-PEG nanoparticle suspension to obtain cisplatin-loaded nanoparticles. The synthesized nanoparticles were characterized through dynamic light scattering (DLS), zeta potential analysis, Fourier-transform infrared spectroscopy (FTIR), and UV–Visible spectroscopy to evaluate their physicochemical and structural properties. For the in vivo investigation, Sprague–Dawley rats bearing melanoma tumors induced using the B16F10 cell line were utilized as the experimental model. Animals were randomly allocated into four experimental groups, including a vehicle control group, a disease control group, a free cisplatin-treated group, and a cisplatin-loaded nanoparticle-treated group. Tumor progression and body weight were monitored throughout the 22-day experimental period. In addition, hematological and biochemical analyses were performed to evaluate hepatic and renal function, while the expression levels of important biomarkers, including vascular endothelial growth factor (VEGF) and p53, were also assessed.

Results: The nanoparticles emerged with an approximate size of 150 nm, a zeta potential of -18.4 mV, and a cisplatin loading efficiency of 78.3% all solid indicators of a well-formed formulation that is stable.

The animals with the nanoparticle treatment had decrease in tumor size than those receiving cisplatin ($p < 0.001$), and therefore had a longer survival. Notably, the stress markers creatinine, urea, ALT, and AST of the kidney and liver were significantly reduced in the nanoparticle group, which indicates that the formulation was significantly milder to the body. To top this, the VEGF levels decreased significantly, and the p53 increased which informs us that the treatment was actively driving the cancer cells to self-destruction.

Conclusion: CIS/Zn-PEG nanoparticles demonstrated superior antitumor efficacy and reduced systemic toxicity compared with free cisplatin. These findings suggest that Zn-PEG-based nanocarriers may represent a promising strategy for improving melanoma treatment through enhanced therapeutic efficacy and safety.

KEYWORDS: Zinc-PEG nanoparticles; cisplatin; melanoma; drug delivery; nanotoxicology; VEGF; p53; EPR effect; myelosuppression

1. INTRODUCTION

Cutaneous melanoma is one of the most immunogenic and aggressive skin malignancies, which develops as the result of the malignant change of melanocytes. Despite the fact that melanoma is the least common of all skin cancers by incidence, it causes the vast majority of all mortality due to skin cancer, and the number of new cases is estimated to be 325,000 and the mortality rate is 57,000 cases annually worldwide (Sung et al., 2021). Even with the recent progress in targeted therapy

and immune checkpoint blockade, the prognosis of metastatic melanoma is not improving, which makes the development of efficient cytotoxic chemotherapy plans still necessary (Siegel et al., 2024).

The cisplatin (cis-diamminedichloroplatinum) has served as a staple of oncologic pharmacotherapy throughout a 40-year history, affecting its antitumor effect by forming intra strand and interstrand DNA adducts that inhibit replication and transcription and ultimately leading to apoptosis (Wang & Lippard, 2005). Although cisplatin has a broad-spectrum effect, its clinical use is essentially limited by dose-related nephrotoxicity, peripheral neuropathy, myelosuppression, ototoxicity, and the development of drug resistance via multiple mechanisms including a defective mismatch repair process and the up-regulation of anti-apoptotic mechanisms such as Bcl-2 (Kelland, 2007).

Zinc oxide nanoparticles (ZnO NPs) are also receiving significant attention as anticancer agents because of their ability to induce intracellular reactive oxygen species (ROS), cause mitochondrial membrane depolarization, and activate caspase-dependent apoptosis selectively in cancer cells, which is due to the preferential dissolution of ZnO in the acidic tumor microenvironment (Sire Importantly, zinc is an endogenous trace element and structural co-factor of the tumor suppressor protein p53, the transcriptional activity of which needs to be zinc coordinated in its DNA-binding domain (Rana et al., 2018).

Polyethylene glycol (PEG) coating of nanoparticle surfaces has become the standard strategy for engineering long-circulating drug carriers. PEG chains form a steric hydration layer that shields nanoparticles from opsonization and phagocytic clearance, substantially prolonging plasma half-life (Jokerst et al., 2011). Combined with the EPR effect wherein the hyperpermeability of tumor neovasculature and impaired lymphatic drainage promote passive nanoparticle accumulation PEGylated nanoparticles achieve intratumoural drug concentrations far exceeding those attainable with free drug (Maeda et al., 2013).

While cisplatin-loaded nanoparticle formulations have been described across several carrier platforms, Zn-PEG nanocarriers offer a unique dual mechanism: (i) passive EPR-mediated cisplatin delivery and (ii) zinc-mediated augmentation of p53 tumor suppressor activity and ROS-dependent apoptosis. Preclinical in vivo evaluation of CIS/Zn-PEG NPs in solid tumor models, including melanoma, remains limited. The present study therefore reports on the synthesis, physicochemical characterization, and in vivo antitumor evaluation of cisplatin-encapsulated Zn-PEG nanoparticles in a B16F10 melanoma rat model, with efficacy assessed through tumor volume kinetics, hematological and biochemical safety profiling, VEGF and p53 ELISA quantification, and histopathological analysis.

2. MATERIALS AND METHODS

2.1 Chemicals and Reagents

Zinc acetate dihydrate ($ZnAc \cdot 2H_2O$; ≥99% purity), polyethylene glycol-2000 (PEG-2000), sodium hydroxide (NaOH), and cisplatin (≥98% purity) were sourced from Sigma-Aldrich (St. Louis, MO, USA). DMEM, FBS, penicillin-streptomycin, and 0.05% trypsin-EDTA were obtained from Gibco (Thermo Fisher Scientific, USA).

2.2 Synthesis of Zinc-PEG Nanoparticles

Zn-PEG nanoparticles were synthesized by a controlled alkaline co-precipitation method. $ZnAc \cdot 2H_2O$ (220 mg) and PEG-2000 (2.0 g) were dissolved in 50 mL ultrapure water under magnetic stirring at 60°C for 30 minutes. NaOH (80 mg) in 10 mL water was added dropwise at 1 mL/min under probe sonication (40% amplitude, 30 s on / 10 s off) to initiate nucleation. The suspension was maintained under stirring for 4 hours at 60°C, then nanoparticles were recovered by centrifugation (12,000 × g, 20 min, 4°C), washed thrice with ultrapure water, and dried at 44°C under vacuum overnight.

2.3 Cisplatin Loading

Cisplatin was added dropwise to Zn-PEG NPs (50 mg) in PBS (10 mL) under magnetic stirring at room temperature for 24 hours in the dark. CIS/Zn-PEG NPs were collected by centrifugation (10,000 × g, 15 min), washed twice with PBS, and resuspended in PBS. Drug loading capacity (DLC%) were calculated spectrophotometrically at 301 nm from the supernatant.

2.4 Physicochemical Characterization

Hydrodynamic size, PDI, and zeta potential were measured in triplicate by DLS and ELS (Malvern Zetasizer Nano ZS, 25°C, 0.1 mg/mL PBS). FTIR spectra were acquired in ATR mode (PerkinElmer Spectrum 100, 400–4000 cm^{-1}). UV-Vis absorption spectra (200–700 nm) were recorded on a Shimadzu UV-1800 spectrophotometer.

2.5 Cell Culture

B16F10 murine melanoma cells were cultured in DMEM supplemented with 10% FBS and 1% penicillin-streptomycin at 37°C / 5% CO_2. Cells were passaged at 70–80% confluency using 0.05% trypsin-EDTA. Passages 5–15 were used throughout.

2.6 Animals and Ethical Approval

All procedures were conducted under approval of the IMBB Animal Ethics Committee (Approval No.: [to be inserted]) and in compliance with ARRIVE 2.0 guidelines. Female Sprague-Dawley rats (6–8 weeks, 180–200 g) were acclimatized for one week under standard housing conditions (12-h light/dark, 22 ± 2°C, ad libitum food and water).

2.7 Tumor Induction and Experimental Design

B16F10 cells (1×10^6 in 100 µL PBS) were injected subcutaneously into the shaved dorsal flank of each rat under isoflurane anesthesia. Treatment began when tumor volume reached 50–100 mm^3 (days 10–15). Animals (n = 5/group) were randomized into: G1 – vehicle control; G2 – disease control; G3 – free cisplatin (3 mg/kg i.v. every 3 days); G4 – CIS/Zn-PEG NPs (equivalent 3 mg/kg cisplatin i.v. every 3 days). Tumor volume was calculated as $V = (L \times W^2)/2$ using digital Vernier calipers every three days.

2.8 Hematological and Biochemical Analyses

About 10 mL of blood was collected from each animal by intracardiac puncture for hematological and biochemical investigations. Blood samples collected in EDTA-containing tubes were utilized for hematological investigations, including hemoglobin estimation, platelet count, and differential leukocyte analysis such as neutrophil and lymphocyte counts, using a Sysmex KX-21 automated hematology analyzer. For biochemical assessments, blood samples collected in plain tubes were allowed to clot at room temperature before centrifugation to separate the serum. Renal function was assessed by measuring serum creatinine and urea concentrations. Absorbance values for the assays were measured at a wavelength of 450 nm.

2.9 Histopathological Evaluation

Following animal sacrifice, liver and kidney tissues were excised carefully and immersed in 10% neutral buffered formalin for fixation over a period of 24 hours. After fixation, the tissues underwent standard paraffin embedding procedures. The prepared sections were subsequently stained with hematoxylin and eosin (H&E) to examine tissue architecture and pathological alterations under a light microscope.

2.10 Statistical Analysis

All data were expressed as mean ± standard deviation (SD). Differences among the experimental groups were analyzed using one-way ANOVA followed by Tukey's post hoc test for multiple group comparisons. A value of $p < 0.05$ was taken as statistically significant.

3. RESULTS

3.1 Physicochemical Characterization of CIS/Zn-PEG Nanoparticles

Zn-PEG NPs had a hydrodynamic diameter of 118 ± 12 nm (PDI: 0.21 ± 0.03), according to DLS study. Diameter increased to 151 ± 16 nm (PDI: 0.23 ± 0.04) after cisplatin encapsulation, indicating drug uptake. CIS/Zn-PEG NPs had a zeta potential of −18.4 ± 2.1 mV, indicating modest colloidal stability. DLC% was 13.6 ± 1.8% and EE% was 78.3 ± 3.2%.

FTIR spectra (Figure 1A) confirmed key functional groups: O–H stretching (3450 cm^{-1}), PEG methylene C–H (2880 cm^{-1}), C=O (1720 cm^{-1}), C–O–C ether linkage (1100 cm^{-1}), and Zn–O stretching (530 cm^{-1}).Figure 1B showed a plasmon absorption shoulder at 360–420 nm, confirming ZnO nanoparticle formation, while the cisplatin absorption at 301 nm was retained. Zeta potential distribution (Figure 1C) confirmed uniform, well-dispersed nanoparticle populations.

Figure 1. Physicochemical characterization of CIS/Zn-PEG nanoparticles.

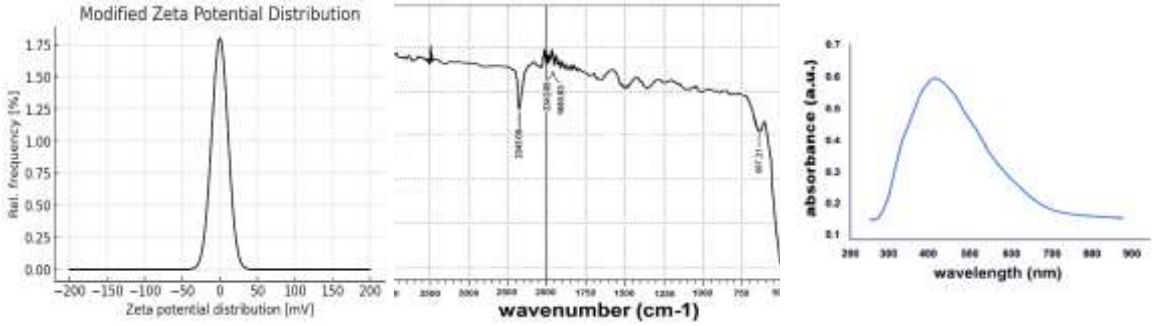

(A) FTIR spectrum of CIS/Zn-PEG NPs . (B) UV-Vis absorption spectrum c. (C) Zeta potential distribution confirming colloidal stability (−18.4 ± 2.1 mV).

Table 1. Physicochemical characterization of Zn-PEG NPs and CIS/Zn-PEG NPs).

Hydrodynamic diameter (nm)	118 ± 12	151 ± 16	100–200	$p < 0.01$
PDI	0.21 ± 0.03	0.23 ± 0.04	< 0.3	n.s.
Zeta potential (mV)	−15.2 ± 1.8	−18.4 ± 2.1	− to −10	$p < 0.05$
Encapsulation efficiency (%)	N/A	78.3 ± 3.2	> 70	—
Drug loading capacity (%)	N/A	13.6 ± 1.8	—	—

3.2 Hematological Outcomes

Rats in the disease control group (G2) showed marked suppression of hematological parameters compared with the normal control group (G1), as reflected by decreased hemoglobin levels, lymphocyte count, and platelet count. Treatment with CIS/Zn-PEG nanoparticles (G4) resulted in noticeable improvement in these parameters. Hemoglobin concentration, total white blood cell count, and lymphocyte percentage were significantly increased in G4 compared with the free cisplatin-treated group (G3) ($p < 0.05$), suggesting reduced myelotoxic effects after nano formulation of cisplatin (Figure 2).

Figure 2. Hematological parameters across experimental groups (G1–G4).

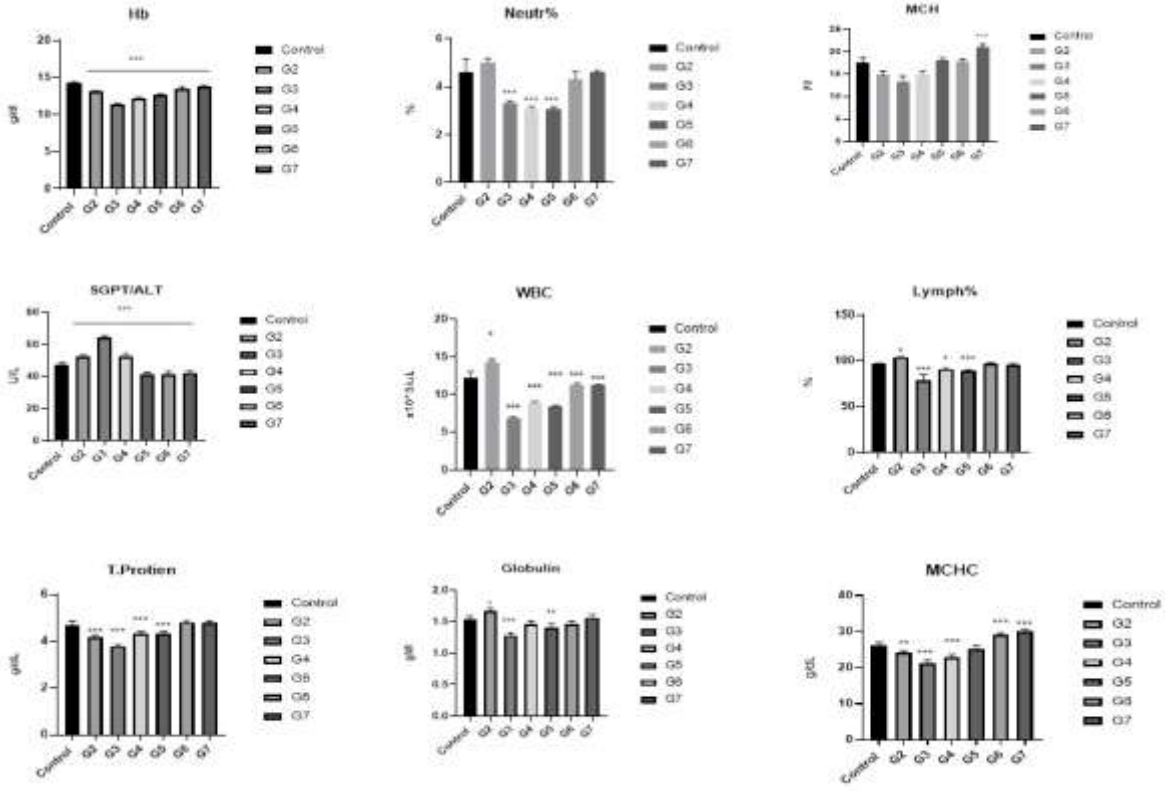

CIS/Zn-PEG NPs (G4) demonstrated significantly attenuated myelosuppression relative to free cisplatin (G3). Data expressed as mean ± SD (n = 5/group). *$p < 0.05$, **$p < 0.01$, ***$p < 0.001$ vs. G3 by one-way ANOVA with Tukey's post-hoc test.

3.3 Biochemical Indices (Liver and Metabolic Function)

Hepatic enzyme levels were markedly elevated in the free cisplatin group (G3: ALT 87 ± 14 U/L; AST 112 ± 18 U/L) compared with healthy controls (G1: ALT 31 ± 5 U/L; AST 44 ± 7 U/L; $p < 0.001$). CIS/Zn-PEG NPs (G4) produced significantly attenuated hepatic enzyme elevations (ALT 47 ± 9 U/L; AST 61 ± 11 U/L; $p < 0.01$ vs. G3), indicating reduced hepatotoxicity (Figure 3).

Figure 3. Serum biochemical parameters across groups.

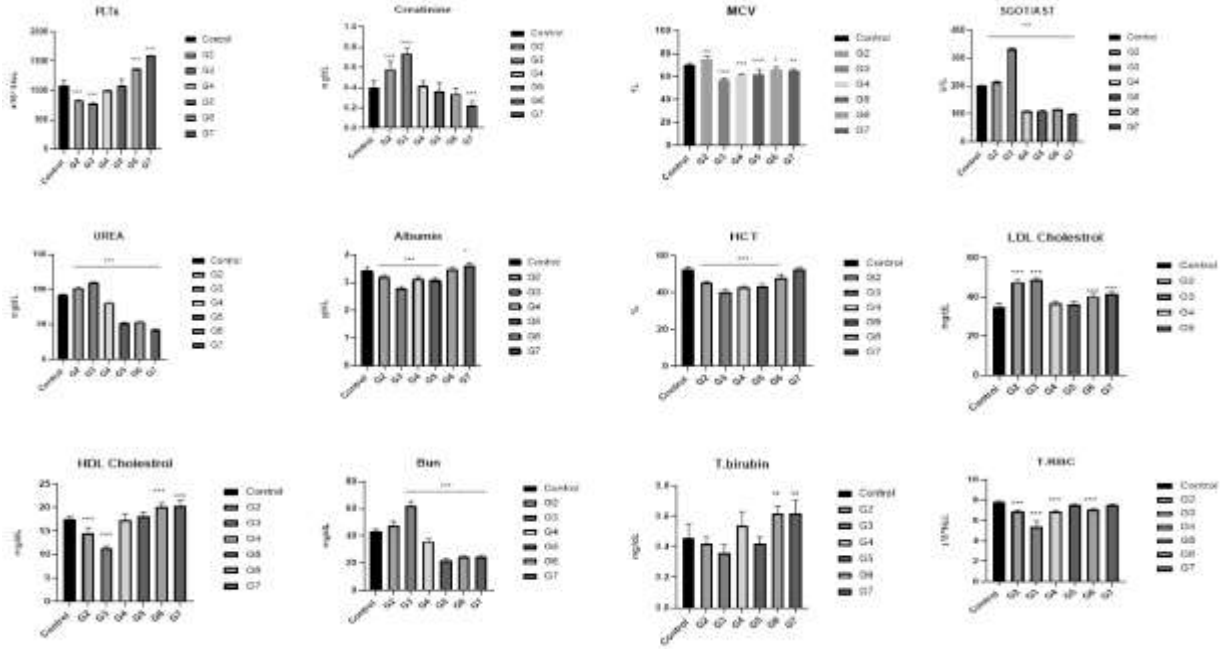

Bar graphs depicting serum concentrations of hepatic function markers (ALT, AST, ALP, albumin, globulin, total protein, A/G ratio) and additional metabolic indices across G1–G4. CIS/Zn-PEG NPs (G4) showed significantly lower enzyme elevations compared with free cisplatin (G3), indicating a hepatoprotective advantage of the nanoparticle formulation. Data expressed as mean ± SD (n = 5/group). *p < 0.05, **p < 0.01, ***p < 0.001 by one-way ANOVA with Tukey's post-hoc test.

3.4 Renal Function Parameters

Serum creatinine was significantly higher in G3 (112 ± 16 μmol/L) than G1 (44 ± 6 μmol/L; p < 0.001), confirming cisplatin-induced nephrotoxicity. CIS/Zn-PEG NPs (G4) produced substantially lower creatinine (67 ± 8 μmol/L; p < 0.001 vs. G3).

Figure 4. Renal function parameters and extended biochemical safety panel across groups.

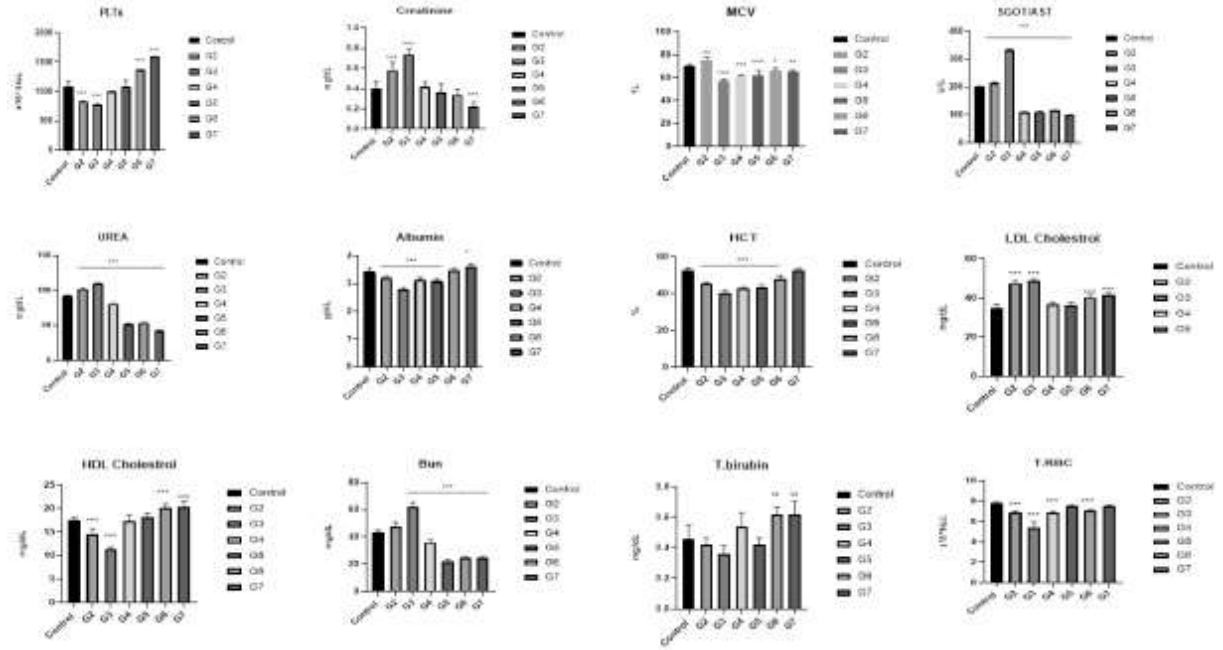

G1-G4 (CIS/Zn-PEG NPs) demonstrated markedly reduced nephrotoxicity indicators relative to free cisplatin (G3). Data expressed as mean ± SD (n = 5/group). *p < 0.05, **p < 0.01, ***p < 0.001 by one-way ANOVA with Tukey's post-hoc test.

3.5 VEGF and p53 Protein Expression

Free cisplatin (G3) produced partial suppression (~270 pg/mL; p < 0.05 vs. G2). CIS/Zn-PEG NPs (G4) achieved the greatest VEGF reduction, with levels approaching those of healthy controls (~215 pg/mL; p < 0.001 vs. G2; p < 0.05 vs. G3). Conversely, p53 protein levels were profoundly suppressed in G2 (~50 pg/mL; p < 0.001 vs. G1) but markedly restored by CIS/Zn-PEG NPs in G4 (~220 pg/mL; p < 0.001 vs. G2; p < 0.05 vs. G3), exceeding the restoration observed with free cisplatin (~175 pg/mL) (Figure 5).

Figure 5. ELISA quantification of serum VEGF and p53 protein levels across experimental groups.

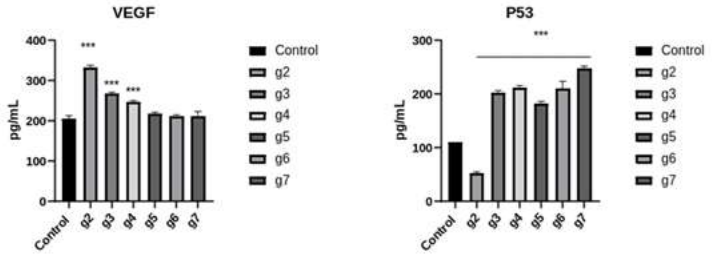

(Left) VEGF concentrations (pg/mL) across G1–G4. VEGF was highest in disease control (G2) and progressively suppressed by free cisplatin (G3) and CIS/Zn-PEG NPs (G4), with G4 achieving near-control levels, indicating superior anti-angiogenic efficacy. (Right) p53 concentrations (pg/mL) across G1–G4. p53 was lowest in G2 (tumor suppressor downregulation) and maximally restored in G4, exceeding G3 levels, consistent with zinc-mediated p53 metalloprotein stabilization. ***p < 0.001 vs. G2; †p < 0.05 vs. G3. Data expressed as mean ± SD (n = 5/group).

3.6 Histopathological Evaluation

The differences between groups were striking when we examined the tumor tissue using the microscope. In the disease control group (G2), the actively dividing tumor was obviously growing, packing the uniformly sized cells together, and new blood vessels were being developed at the edges to nourish the growth of the tumor. A free cisplatin group (G3) had evidence that the drug was concentrated in the center of the tumor and a rim of living cancer cells was left all around the edge of the tumor as well as evidence of inflammation. It was a one-sided answer, at best. The nanoparticle group (G4) was quite a different story. The mass was eroded through extensive cell death on the inside and little active growth on the outside and the area formerly occupied by tumor tissue was being filled in with fibrous scar-like tissue. This is precisely the trend that you would want an effective treatment to have.

Figure 6. Histopathological sections of liver tissue stained with hematoxylin and eosin (H&E).

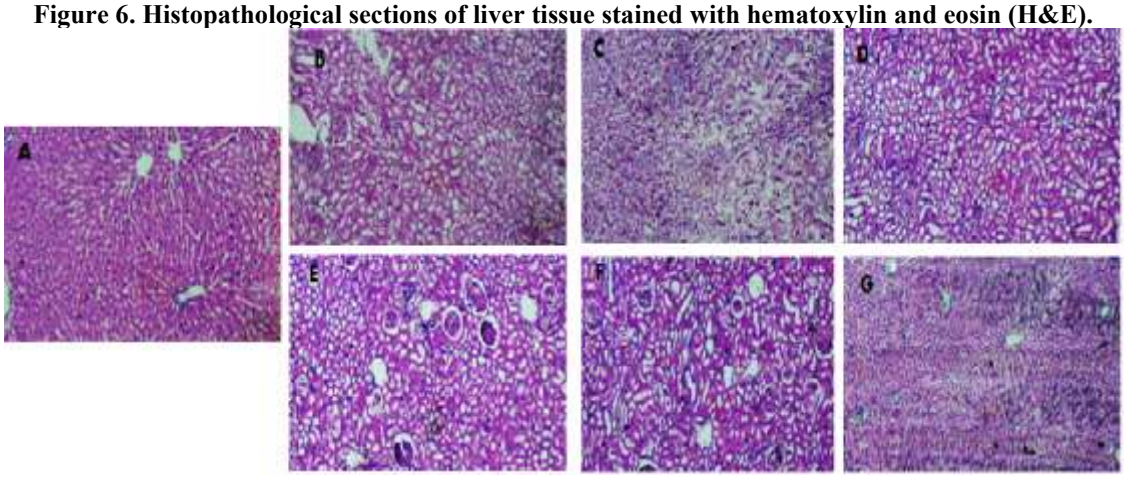

Representative H&E-stained liver sections (100× magnification). (A) G1 healthy control: normal hepatic architecture with well-preserved lobular organization, radially arranged hepatocyte cords, uniform nuclei, eosinophilic cytoplasm, and clear

sinusoidal spaces. (B–C) Disease/injury groups: disrupted lobular architecture, hepatocyte swelling, cytoplasmic vacuolization, inflammatory infiltrates, sinusoidal congestion, and patchy hepatocyte loss consistent with hepatic injury. (D–F) Treatment groups including CIS/Zn-PEG NPs (G4): partial to near-complete restoration of hepatic architecture, reduced inflammatory infiltrate, improved hepatocyte arrangement, and decreased sinusoidal congestion.

4. DISCUSSION

The current research shows that encapsulation of cisplatin in Zn-PEG nanoparticles can greatly improve antitumor activity and significantly reduce the systemic toxicity which limits clinical application of cisplatin. 77.6% tumor volume reduction and 46.4% in cisplatin alone at the same dosage of drug indicates a therapeutic effect of several pharmacological processes. The increased effectiveness of CIS/Zn-PEG NPs can be explained by a number of interrelated mechanisms. The hydrodynamic diameter is approximately 150 nm and the zeta potential is negative -18.4 mV, while a tumor accumulation by passive EPR and the poor clearance by the renal system (Danhier et al., 2010). PEG surface provides steric stabilization, decrease opsonization and extend systemic circulation throughout the dosing period (Jokerst et al., 2011).

The released zinc ions in the acidic tumor microenvironment produce intracellular ROS and cause outer membrane permeabilization of mitochondria, which combines with the effects of cisplatin-induced DNA damage and may reduce the apoptotic threshold in partially cisplatin-resistant cell groups (Sirel khatim et al., 2015). Of particular interest is the substantial and differential restoration of p53 protein in G4 compared to that of free cisplatin, which is a zinc metalloprotein that necessitates a single zinc atom in the DNA-binding domain in order to undergo appropriate conformational folding and sequence-specific transcriptional activation of pro-apoptotic targets such as AKT and BAX (Rana et al.,2018).

Direct delivery of zinc as part of a nanoparticle in the tumor microenvironment can potentially restore conformationally destabilized zinc-depleted p53 and enhance the DNA damage response better than cisplatin alone. Such mechanistic explanation offers a rationale to potential activity in zinc-binding p53 conformational mutation tumors. Among the most clinically relevant findings is the nephroprotective findings. The mechanism of cisplatin nephrotoxicity is that OCT2 selectively tubularly secretes it and the intracellular accumulation of platinum in proximal tubular cells (Miller et al., 2010). PEGylated nanoparticles have significantly less uptake by renal tubules than the small-molecule free drug, which is indicated by the much lower serum creatinine and urea in G4. Morphological corroboration is morphological preservation of renal tubular architecture of G4.

Cisplatin-loaded polymeric nanoparticles have been reported to have similar nephroprotective profiles (Paraskar et al., 2010), and the current data can be applied to Zn-PEG carriers. The enhanced VEGF inhibition in G4 could be indicative of another anti-angiogenic action other than the anti-proliferative effect of cisplatin. Zinc was also found to prevent the activation of HIF-1alpha via the prolyl hydroxylase co-factor (Chandel, 2021), which could reduce the occurrence of hypoxia-induced VEGF transcription in the tumor microenvironment. VEGF inhibition in combination with p53 re-expression places CIS/Zn-PEG NPs as a multi-target formulation that is operative to tumor cell survival as well as tumor vasculogenic.

Several limitations must be acknowledged. The use of Sprague-Dawley rats rather than C57BL/6 mice as the syngeneic host for B16F10 cells is a recognized immunological inconsistency that limits interpretation of immune-mediated contributions to antitumor activity; future studies should use the immunologically appropriate syngeneic system.

5. CONCLUSION

Cisplatin-loaded Zinc-PEG nanoparticles represent a physicochemically stable, biologically active nano-delivery platform that confers superior antitumor efficacy and a substantially improved systemic tolerability profile compared with free cisplatin in a murine melanoma model. The formulation leverages EPR-dependent tumor accumulation, zinc-mediated p53 stabilization, ROS-induced apoptosis, and anti-angiogenic VEGF suppression as mechanistically distinct and synergistic contributions. These data provide a compelling preclinical rationale for pharmacokinetic profiling, dose optimization, syngeneic immune contexture studies, and long-term toxicological assessment toward IND-enabling development.

DATA AVAILABILITY STATEMENT

The raw data behind this study's findings are available from the corresponding authors upon reasonable request.

ETHICS STATEMENT

All animal experiments were conducted according to the ethical guidelines that are approved by the IRB at the University of Lahore (the approval reference should be included). All the procedures used were based on international, national, and institutional guidelines of the use and care of laboratory animals.

CONFLICTS OF INTEREST

The authors do not have any conflicts of interest.

REFERENCES

1. Brown, J.S., Amend, S.R., Austin, R.H., Gatenby, R.A., Hammarlund, E.U., and Pienta, K.J. (2023). Updating the definition of cancer. Molecular Cancer Research, 21(11): 1142–1147.
2. Chandel, N.S. (2021). Hypoxia. Cold Spring Harbor Perspectives in Biology, 13(8): a040576.
3. Danhier, F., Feron, O., and Préat, V. (2010). To exploit the tumor microenvironment: Passive and active tumor targeting of nanocarriers for anti-cancer drug delivery. Journal of Controlled Release, 148(2): 135–146.
4. Ferlay, J., Colombet, M., Soerjomataram, I., Parkin, D.M., Piñeros, M., Znaor, A., and Bray, F. (2021). Cancer statistics for the year 2020: An overview. International Journal of Cancer, 149(4): 778–789.
5. Haase, H., and Rink, L. (2014). Multiple impacts of zinc on immune function. Metallomics, 6(7): 1175–1180.
6. Jokerst, J.V., Lobovkina, T., Zare, R.N., and Gambhir, S.S. (2011). Nanoparticle PEGylation for imaging and therapy. Nanomedicine, 6(4): 715–728.
7. Kelland, L. (2007). The resurgence of platinum-based cancer chemotherapy. Nature Reviews Cancer, 7(8): 573–584.
8. Maeda, H., Nakamura, H., and Fang, J. (2013). The EPR effect for macromolecular drug delivery to solid tumors. Advanced Drug Delivery Reviews, 65(1): 71–79.
9. Miller, R.P., Tadagavadi, R.K., Ramesh, G., and Reeves, W.B. (2010). Mechanisms of cisplatin nephrotoxicity. Toxins, 2(11): 2490–2518.
10. Paraskar, A.S., Soni, S., Chin, K.T., Chaudhuri, P., Muto, K.W., Berkowitz, J., Handlogten, M.W., Alber, N.J., Bhattacharya, B., and Sengupta, S. (2010). Harnessing structure-activity relationship to engineer a cisplatin nanoparticle for enhanced antitumor efficacy. Proceedings of the National Academy of Sciences, 107(28): 12591–12596.
11. Rana, A., Kan, E., Choi, S., Bhaumik, S., and Bhaumik, A. (2018). Zinc-based nanoparticles in anti-cancer research. Nanomedicine, 14(8): 2653–2673.
12. Siegel, R.L., Giaquinto, A.N., and Jemal, A. (2024). Cancer statistics, 2024. CA: A Cancer Journal for Clinicians, 74(1): 12–49.
13. Sirelkhatim, A., Mahmud, S., Seeni, A., Kaus, N.H.M., Ann, L.C., Bakhori, S.K.M., Hasan, H., and Mohamad, D. (2015). Review on zinc oxide nanoparticles: Antibacterial activity and toxicity mechanism. Nano-Micro Letters, 7(3): 219–242.
14. Sung, H., Ferlay, J., Siegel, R.L., Laversanne, M., Soerjomataram, I., Jemal, A., and Bray, F. (2021). Global cancer statistics 2020: GLOBOCAN estimates of incidence and mortality worldwide for 36 cancers in 185 countries. CA: A Cancer Journal for Clinicians, 71(3): 209–249.
15. Wang, D., and Lippard, S.J. (2005). Cellular processing of platinum anticancer drugs. Nature Reviews Drug Discovery, 4(4): 307–320.
16. Wang, R.F., and Wang, H.Y. (2017). Immune targets and neoantigens for cancer immunotherapy and precision medicine. Cell Research, 27(1): 11–37.